

# Spherical Assemblies from $\pi$ -Conjugated Alternating Copolymers: Toward Optoelectronic Colloidal Crystals

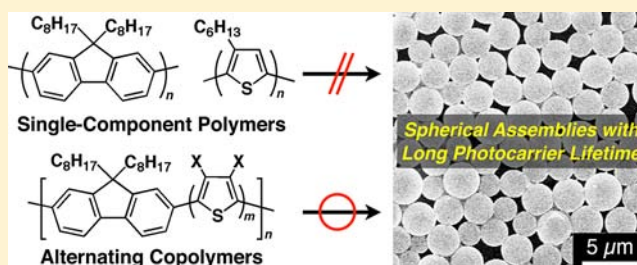
Taeko Adachi,<sup>†</sup> Liang Tong,<sup>†</sup> Junpei Kuwabara,<sup>†,‡</sup> Takaki Kanbara,<sup>†,‡</sup> Akinori Saeki,<sup>§</sup> Shu Seki,<sup>§</sup> and Yohei Yamamoto<sup>\*,†,‡</sup>

<sup>†</sup>Division of Materials Science, and <sup>‡</sup>Tsukuba Research Center for Interdisciplinary Materials Science (TIMS), Faculty of Pure and Applied Sciences, University of Tsukuba, 1-1-1 Tennodai, Tsukuba, Ibaraki 305-8573, Japan

<sup>§</sup>Department of Applied Chemistry, Graduate School of Engineering, Osaka University, 2-1 Yamadaoka, Suita, Osaka 565-0871, Japan

## S Supporting Information

**ABSTRACT:** Self-assembly of conducting polymers, which are often used as photoabsorbing, charge-transporting, and photoemission layers of organic photovoltaic and light-emitting devices, were comprehensively studied by means of slow precipitation from polymer solutions upon addition of a vapor of nonsolvents. Polymers such as polyfluorene and polythiophene having a single monomer component hardly formed defined and discrete objects but only gave ill-defined aggregates. In contrast, alternating copolymers typically having both fluorene and thiophene components in their repeating unit self-assembled into well-shaped spheres with diameters ranging from several hundreds of nanometers to several micrometers. Such clear differences in terms of the assembling geometries derive from the rigidity and crystallinity of the polymers, where the copolymers possess large steric hindrance on their backbone that reduces planarity of the polymers and inhibits anisotropic crystal growth, leading to the formation of structurally isotropic spheres. Changing the assembling parameters can systematically control diameter and deviation of the spheres. Furthermore, photocarrier lifetimes of the spheres were markedly enhanced by more than 3 orders of magnitude in comparison with those of cast films from their solutions. This research gives a useful guide for preparation of colloidal crystals from  $\pi$ -conjugated polymers toward their optoelectronic applications.



## 1. INTRODUCTION

Integration of polymer beads having a size comparable to the wavelength of visible-to-ultraviolet light creates three-dimensional (3D) colloidal crystals that exhibit novel optical properties.<sup>1–5</sup> So far, various colloidal crystals consisting of beads of nonconjugated polymers such as polystyrene (PS) and poly(methyl methacrylate) (PMMA) were reported. These crystals act as photonic crystals, exhibiting optical band gap,<sup>6</sup> nonlinear optics,<sup>7</sup> and laser oscillation.<sup>8</sup> Meanwhile, few examples have been reported on photonic crystals consisting of  $\pi$ -conjugated polymers.<sup>9–12</sup> Examples of  $\pi$ -conjugated polymer photonic crystals include an inverted opal structure of poly(3-alkylthiophene)<sup>9</sup> and poly(*para*-phenylenevinylene) (PPV),<sup>10,11</sup> which are infiltrated into voids of silica or opal colloidal crystals. Another example is also from PPV spheres, prepared by an annealing of colloidal crystal of nonconjugated PPV precursors formed by the so-called self-organized precipitation (SORP) method.<sup>12</sup> Photonic crystals consisting of  $\pi$ -conjugated polymers are expected to show novel optoelectronic properties such as enhanced electroluminescence, no-threshold laser oscillation, and highly efficient photoelectric conversion as the results of charge injection, long-lived excitons, and light confinement.<sup>13,14</sup> Thus, developing a formation of colloidal crystals from  $\pi$ -conjugated

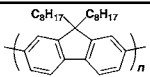
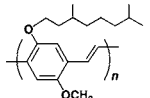
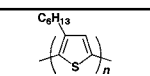
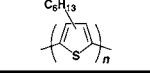
polymers will take great advantages for developing new polymer-based photonic crystals.

In general, polymer colloids are prepared by either direct generation during polymerization from the corresponding monomers (direct polymerization) or secondary generation such as rapid reprecipitation or emulsification of polymers (postpolymerization). The majority of the reported  $\pi$ -conjugated polymer colloids were achieved by the direct polymerization techniques such as dispersion polymerization and miniemulsion polymerization.<sup>15,16</sup> On the other hand, not many examples are reported on spherical assemblies of  $\pi$ -conjugated polymers by postpolymerization,<sup>15</sup> including self-assembly of amphiphilic  $\pi$ -conjugated homopolymers<sup>17</sup> or block copolymers.<sup>18–20</sup> One possible reason  $\pi$ -conjugated polymers have difficulty giving spherical assemblies by postpolymerization is attributed to their high rigidity and crystallinity.<sup>21,22</sup>  $\pi$ -Conjugation makes the polymer backbone planar and rigid, which lowers the flexibility of the polymers in contrast with nonconjugated polymers such as PS and PMMA. As the result of high planarity,  $\pi$ -conjugated polymers tend to stack on one another and crystallize anisotropically, often giving one-dimensional (1D) fibril or two-dimensional (2D) layered

Received: October 30, 2012

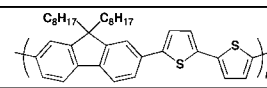
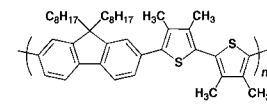
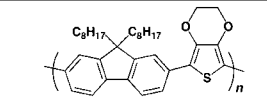
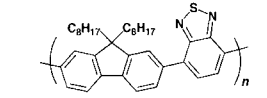
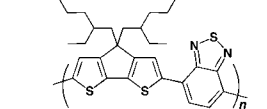
Published: December 28, 2012

Table 1. Summary of Single-Component Polymers, Assembling Condition, Geometry, and Size

Polymer	Chemical Structure	$M_n^a$ , $M_w/M_n^a$ , DP <sup>b</sup>	Solvent/Vapor <sup>c</sup>	Assembling Geometry	$d_{av}$ ( $\sigma$ ) / $\mu\text{m}$	Corresponding Figure and Table
F8		15800, 3.70, 41	Toluene /Acetone	Distorted and Fused Spheres	0.9–1.9	Figure S2 Table S1
MDMOPPV		23000, –, 80	CH <sub>2</sub> Cl <sub>2</sub> /MeOH	Distorted and Fused Spheres	1.1–2.8	Figure S3 Table S2
RR-P3HT (regioregular)		17500, –, 105	CHCl <sub>3</sub> /Acetone	Irregular Aggregates	–	Figure S4 Table S3
rr-P3HT (regiorandom)		29200, 3.16, 175	CHCl <sub>3</sub> /MeOH	Fused Spheres	1.8 (0.61)	Figure S5 Table S4

<sup>a</sup>Estimated by gel permeation chromatography (GPC) calibrated on polystyrene standards or reported by company. <sup>b</sup>Average degree of polymerization (DP), calculated from  $M_n$  and molecular weight of the repeating unit. <sup>c</sup>Initial concentration and assembling temperature were 1 mg mL<sup>-1</sup> and 25 °C, respectively.

Table 2. Summary of Alternating Copolymers, Assembling Conditions, Geometry, and Size

Polymer	Chemical Structure	$M_n^a$ , $M_w/M_n^a$ , DP <sup>b</sup>	Solvent/Vapor <sup>c</sup>	Assembling Geometry	$d_{av}$ ( $\sigma$ ) / $\mu\text{m}$	Corresponding Figure and Table
F8T2		26600, 2.66, 48	CHCl <sub>3</sub> /MeOH	Irregular Aggregates	–	Figure S6 Table S5
F8TMT2		31800, 2.46, 52	CH <sub>2</sub> Cl <sub>2</sub> /MeOH CHCl <sub>3</sub> /MeOH THF/MeOH CHCl <sub>3</sub> /Acetone CH <sub>2</sub> Cl <sub>2</sub> /Acetone	Well-Shaped Spheres	2.7 (0.39) 2.4 (1.2) 1.9 (0.73) 1.5 (0.61) 1.9 (0.59)	Figure 1, Table 3
F8EDOT		27000, 3.81, 51 13800, 2.03, 26 6300, 1.43, 12	CHCl <sub>3</sub> /MeOH	Well-Shaped Spheres	0.61 (0.18) 0.44 (0.09) <sup>d</sup> 2.2 (0.78) 4.5 (2.1)	Figure 2, Table 4 Figure 4 Figure S10b Figure S10a
F8BT		10000–20000, <3, 18–36	CHCl <sub>3</sub> /Acetone	Distorted Spheres and Irregular Aggregates	4.2–7.8	Figure S8 Table S6
PCPDTBT		7000–20000, –, 13–37	CHCl <sub>3</sub> /MeOH	Well-Shaped Spheres and Irregular Aggregates	4.5 (0.55)	Figure S9 Table S7

<sup>a</sup>Estimated by gel permeation chromatography (GPC) calibrated on polystyrene standards or reported by company. <sup>b</sup>Average degree of polymerization (DP), calculated from  $M_n$  and molecular weight of the repeating unit. <sup>c</sup>Initial concentration and assembling temperature were 1 mg mL<sup>-1</sup> and 25 °C, respectively. <sup>d</sup>Sample was prepared in a wide-mouth Petri dish.

structures,<sup>21–24</sup> not structurally isotropic spheres. Accordingly, one strategy for obtaining spherical assembly from  $\pi$ -conjugated polymers is to reduce the crystallinity, while without diminishing their electronic properties taking into consideration their optoelectronic applications.

In this Article, we attempted preparation of spherical assemblies from  $\pi$ -conjugated polymers by a slow precipitation from its solution upon addition of a vapor of nonsolvents. Precipitation mechanism of the vapor diffusion method is almost similar to the SORP method, in which the solvent is slowly evaporated from the polymer solution containing both “good” and “poor” solvents. In the SORP method, however, combination of the solvents is limited; poor solvents must be nonvolatile or have a higher boiling point than the good solvents.<sup>12</sup> Meanwhile, vapor diffusion method allows various combinations of the solvents including those having similar boiling points. We noticed that, by the vapor diffusion method,

$\pi$ -conjugated polymers having a single monomer component have difficulty forming well-defined spherical structures. In contrast, several alternating copolymers having two different  $\pi$ -conjugated molecular components tend to form quite well-shaped spheres quantitatively with diameters ranging from a few hundreds of nanometers to several micrometers depending on the self-assembling condition. Interestingly, photocarrier lifetimes were remarkably elongated by the formation of spherical geometries.

## 2. MATERIALS AND METHODS

In this research, four single-component polymers and five multi-component alternating copolymers were used (Tables 1 and 2, respectively). Single-component polymers, poly(9,9-di-*n*-octylfluorenyl-2,7-diyl) (F8, number-average molecular weight,  $M_n$  = 15 800, weight-average molecular weight,  $M_w$  = 58 200, polydispersity index,  $M_w/M_n$  = 3.70), poly[2-methoxy-5-(3,7-dimethyloctyloxy)-1,4-phenyl-

enevinylene] (MDMOPPV,  $M_n = 23\,000$ ), and regioregular (RR)- and regiorandom (rr) poly(3-hexylthiophene-2,5-diyl) (RR-P3HT,  $M_n = 17\,500$ ; rr-P3HT,  $M_n = 29\,200$ ,  $M_w = 92\,300$ ,  $M_w/M_n = 3.16$ ), and alternating copolymers, poly[(9,9-di-*n*-octylfluorenyl-2,7-diyl)-*alt*-(benzo[2,1,3]thiadiazole-4,8-diyl)] (F8BT,  $M_n = 10\,000$ – $20\,000$ ) and poly[2,6-(4,4-bis-(2-ethylhexyl)-4*H*-cyclopenta[2,1-*b*;3,4-*b'*]-bithiophene)-*alt*-4,7-(2,1,3-benzothiadiazole)] (PCPDTBT,  $M_n = 7000$ – $20\,000$ ) were purchased from Aldrich Chemical Co. Ltd. Synthesis of an alternating copolymer, poly[(9,9-dioctylfluorenyl-2,7-diyl)-*alt*-(bithiophene-2,5'-diyl)] (F8T2;  $M_n = 36\,500$ ,  $M_w = 270\,800$ ,  $M_w/M_n = 7.42$ ), was described in the Supporting Information. Alternating copolymers, poly[(9,9-dioctylfluorenyl-2,7-diyl)-*alt*-(3,3',4,4'-tetramethylbithiophene-2,5'-diyl)] (F8TMT2,  $M_n = 31\,800$ ,  $M_w = 78\,200$ ,  $M_w/M_n = 2.46$ ) and poly[(9,9-dioctylfluorenyl-2,7-diyl)-*alt*-(3,4-ethylenedioxythiophene-2,5-diyl)] (F8EDOT, ( $M_n = 27\,000$ ,  $M_w = 102\,900$ ,  $M_w/M_n = 3.81$ ), ( $M_n = 13\,800$ ,  $M_w = 28\,100$ ,  $M_w/M_n = 2.03$ ), and ( $M_n = 6300$ ,  $M_w = 9000$ ,  $M_w/M_n = 1.43$ )), were synthesized according to reported procedures.<sup>25,26</sup> For the preparation of self-assembled precipitates, typically a 5 mL glass vial containing a solution of polymers ( $1\text{ mg mL}^{-1}$ , 2 mL) was placed in a 50 mL glass vial containing 5 mL of a poor solvent to allow for vapor diffusion (Figure S1).  $\text{CHCl}_3$ ,  $\text{CH}_2\text{Cl}_2$ , chlorobenzene (PhCl), tetrahydrofuran (THF), and toluene were used for polymer solution, while methanol (MeOH), acetone, and hexane were used as nonsolvents. While the mixture was kept at 25 °C for 72 h, the solution turned into a suspension. Morphology of the precipitates was observed by scanning electron microscopy (SEM). Optical properties of the spherical precipitates, along with those of the polymer solutions and its drop-cast films, were investigated by photoabsorption, diffuse reflectance, and photoemission spectroscopies. Charge transport properties and photocarrier lifetimes were conducted by an electrodeless method of flash-photolysis time-resolved microwave conductivity (FP-TRMC) measurements<sup>27</sup> using cast films of self-assembled precipitates and those formed from  $\text{CHCl}_3$  solutions.

### 3. RESULTS AND DISCUSSION

**3.1. Self-Assembly of  $\pi$ -Conjugated Polymers.** At first, self-assembly of single-component polymers was investigated. Typical fluorescent polymers, F8 and MDMOPPV,<sup>28</sup> yielded pseudospherical objects from solvent combinations of toluene–acetone (Figure S2) and  $\text{CH}_2\text{Cl}_2$ –MeOH (Figure S3), respectively, but the products were distorted in shape and heavily fused with one another. All of the other combinations of the solvents attempted only gave irregular aggregates or no precipitation (Tables S1 and S2). RR-P3HT, a representative compound for hole-transporting material in bulk heterojunction solar cells,<sup>23,24</sup> gave only irregular aggregates under all solvent conditions examined (Figure S4 and Table S3). On the other hand, rr-P3HT formed spherical structures. However, the yielded spheres were not discrete but heavily fused with one another (Figure S5 and Table S4).

Next, we attempted self-assembly of alternating copolymers. F8T2<sup>29,30</sup> having both fluorene and thiophene moieties in the repeating unit only gave ill-defined aggregates for all solvent conditions attempted (Figure S6 and Table S5). However, of interest, F8TMT2<sup>25</sup> having four methyl groups on the bithiophene unit of F8T2 forms discrete and quite well-shaped spheres. Figure 1a and b shows SEM micrographs of the precipitate formed from  $\text{CH}_2\text{Cl}_2$  solution of F8TMT2 upon diffusion of MeOH vapor, where spherical assemblies formed quantitatively. As shown in the inset of Figure 1b, the average diameter ( $d_{av}$ ) and its standard deviation ( $\sigma$ ) are 2.7 and 0.39  $\mu\text{m}$ , respectively. Different solvent combinations such as  $\text{CHCl}_3$  and THF for good solvents and MeOH and acetone for nonsolvents also afforded spherical assemblies (Figure 1c and d for spheres formed from THF/MeOH combination), but the  $\sigma$

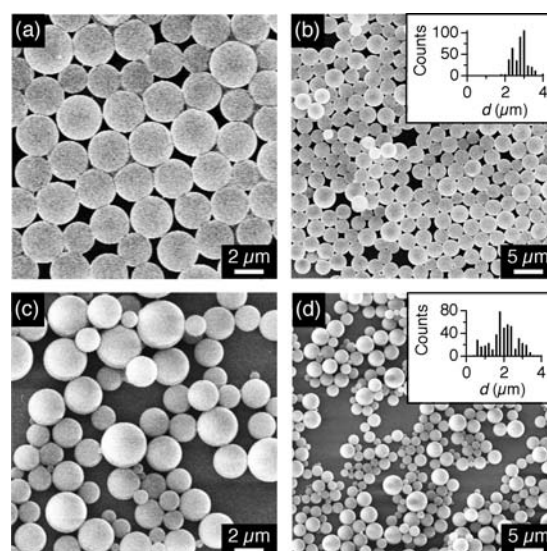


**Figure 1.** SEM micrographs of air-dried  $\text{CH}_2\text{Cl}_2/\text{MeOH}$  (a,b) and THF/MeOH (c,d) suspensions of the spherical assemblies of F8TMT2. Insets in (b) and (d) show histograms of the diameters of the spherical assemblies of F8TMT2, prepared by each condition. The numbers of sample are 407 (b) and 480 (d).

values were larger by 1.5–3 times in comparison with that obtained for a solvent combination of  $\text{CH}_2\text{Cl}_2/\text{MeOH}$  (Table 2). The increase of the deviation is likely derived from the difference of the diffusion rate of the solvents (vide infra). Other solvent combinations only gave ill-defined aggregate or no precipitates (Table 3).

**Table 3. Morphologies of the Self-Assembled Precipitates of F8TMT2 Formed from Each Solvent Combination<sup>a</sup>**

	$\text{CHCl}_3$	$\text{CH}_2\text{Cl}_2$	PhCl	THF	toluene
MeOH	○	○	×	○	×
acetone	○	○	×	△	×
hexane	–	–	–	–	–

<sup>a</sup>○, Well-shaped spheres; △, distorted or fused spheres; ×, irregular aggregates; –, no precipitation.

Similar to F8TMT2, an alternating copolymer, F8EDOT<sup>26</sup> having ethylenedioxythiophene (EDOT) unit instead of tetramethylbithiophene (TMT2) unit, also afforded well-defined spheres with a solvent combination of  $\text{CHCl}_3/\text{MeOH}$  (Figure 2). The  $d_{av}$  and  $\sigma$  values were 610 and 180 nm,

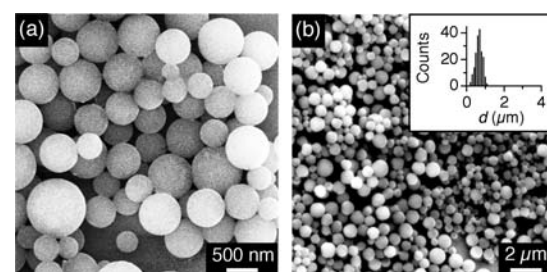


**Figure 2.** SEM micrographs of an air-dried  $\text{CHCl}_3/\text{MeOH}$  suspension of the spherical assemblies of F8EDOT. Inset in (b) shows histogram of the diameters of the spherical assemblies of F8EDOT. The number of sample is 190.



respectively, both of which were remarkably smaller than those formed from **F8TMT2**. Different solvent combinations such as  $\text{CH}_2\text{Cl}_2$  as a good solvent and MeOH, hexane, and acetone as poor solvents also gave spherical assemblies, but they were somewhat distorted or fused with one another (Figure S7). Assemblies in the other solvent combination only gave ill-defined aggregates (Table 4).

**Table 4. Morphologies of the Self-Assembled Precipitates of F8EDOT Formed from Each Solvent Combination<sup>a</sup>**

	$\text{CHCl}_3$	$\text{CH}_2\text{Cl}_2$	PhCl	THF	toluene
MeOH	○	△	×	×	×
acetone	×	△	×	×	×
hexane	△	△	×	×	×

<sup>a</sup>○, Well-shaped spheres; △, distorted or fused spheres; ×, irregular aggregates.

We further investigated other alternating copolymers, **F8BT** and **PCPDTBT**, which are known as donor (D)–acceptor (A) polymers and often used as electron-donating layers of recent polymer photovoltaics.<sup>31–33</sup> These polymers gave mixtures of spheres and irregular aggregates. Spheres of **F8BT** were somewhat distorted with the diameters of 4.2–7.8  $\mu\text{m}$  (Figure S8 and Table S6), while those of **PCPDTBT** were well-shaped with  $d_{\text{av}}$  of 4.5  $\mu\text{m}$  (Figure S9 and Table S7).

**3.2. Size Control of Spherical Assemblies.** For colloidal crystals exhibiting photonic properties at the visible-light region, periodic structure of several hundreds of nanometer is required. The diameter of the spheres formed from **F8EDOT** corresponds to that length scale. Therefore, we used **F8EDOT** and investigated what factor determines the size and deviation of the spheres. Figure 3a shows molecular weight dependence

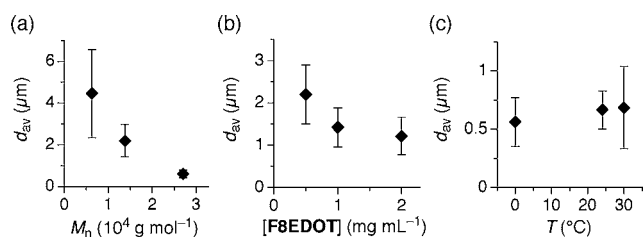


**Figure 3.** Plots of  $d_{\text{av}}$  of the spherical assemblies of **F8EDOT** versus molecular weight (a), initial concentration (b), and assembling temperature (c).

of the diameters of the spheres formed from  $\text{CHCl}_3$  solution of **F8EDOT** upon addition of MeOH vapor. The polymer having  $M_n$  of 27 000 gave spheres with  $d_{\text{av}}$  of 0.61  $\mu\text{m}$ . When  $M_n$  decreased to one-half (13800),  $d_{\text{av}}$  increased to 2.2  $\mu\text{m}$ , and further one-half of  $M_n$  (=6300) resulted in an increase of  $d_{\text{av}}$  to 4.5  $\mu\text{m}$  (Figure S10). Initial concentration of the solution also affects the  $d_{\text{av}}$  values, where  $d_{\text{av}}$  of the resultant spheres decreased from 2.1 to 1.4 and 1.2  $\mu\text{m}$  as the concentration of **F8EDOT** ( $M_n = 27\ 000$ ) was increased from 0.5 to 1.0 and 2.0  $\text{mg mL}^{-1}$ , respectively (Figures 3b and S11). Temperature also affects the sphere size and deviation to some extent, where aging at higher temperature resulted in the larger  $d_{\text{av}}$  values ( $d_{\text{av}}$  of 0.56, 0.67, and 0.69  $\mu\text{m}$  for the spheres assembled at 0, 25, and 30  $^\circ\text{C}$ , respectively; Figures 3c and S12).

The changes of  $d_{\text{av}}$  most likely relate to the rate of precipitation. Because of the high solubility, polymers having

smaller  $M_n$  precipitate with the longer aging time than those having larger  $M_n$ . Accordingly, for the small- $M_n$  polymers, nucleation and growth take place more slowly, leading to the formation of spheres having larger diameters. Low initial concentration also results in slow nucleation and growth of spheres, giving the larger spheres in comparison with that formed from high concentration. Temperature dependency is a little complicated, because solubility is higher at higher temperature, but, at the same time, diffusion of the nonsolvent occurs more rapidly. These factors affect oppositely for the precipitation rate. In the present case, assembly at the higher temperature results in the precipitation of spheres having larger diameters; hence the former (solubility change) is the dominant factor for  $d_{\text{av}}$  of the spheres. According to these results, small-diameter spheres can be obtained by self-assembly of (i) large molecular weight polymers (ii) in high initial concentration (iii) at low temperature. Under such condition, nucleation of polymers occurs concurrently, resulting in a large amount of small-size spheres.

Next, we discuss the deviation of the diameters. Spheres of **F8EDOT** with  $d_{\text{av}}$  of 0.61  $\mu\text{m}$  showed 30% deviation ( $\sigma = 0.18 \mu\text{m}$ ), while those with  $d_{\text{av}}$  of 4.5  $\mu\text{m}$  have the larger deviation of 47% ( $\sigma = 2.1 \mu\text{m}$ , Figure 3a and Table 2). We assume that time lag of the nucleation causes the difference in the growth time of the spheres, thereby resulting in the large deviation of the diameters. In fact, **F8TMT2** in  $\text{CH}_2\text{Cl}_2$ , upon vapor diffusion of MeOH, results in the spherical precipitates with the smaller  $\sigma$  value than that in THF and  $\text{CHCl}_3$  (vide ante), where evaporation of the good solvent takes place more rapidly for  $\text{CH}_2\text{Cl}_2$  than THF and  $\text{CHCl}_3$  (boiling points of  $\text{CH}_2\text{Cl}_2$ , THF, and  $\text{CHCl}_3$  are 40, 66, and 61  $^\circ\text{C}$ , respectively). To reduce the time lag of the nucleation, we further demonstrated self-assemblies using a wide-mouth Petri dish instead of a narrow-mouth vial. Thus, the solution/vapor interface area was increased from 1.5 to 5.7  $\text{cm}^2$ , while the depth of the solution was reduced from 0.8 to 0.2 cm (Figure S13). In this case, a complete precipitation occurred within only 12 h by a vapor diffusion of MeOH into  $\text{CHCl}_3$  solution of **F8EDOT**. As shown in Figure 4,  $d_{\text{av}}$  and  $\sigma$  of the obtained spheres were reduced by 28% and 50%, respectively, from those obtained using usual small-mouth vial ( $d_{\text{av}}$ , 0.61  $\rightarrow$  0.44  $\mu\text{m}$ ;  $\sigma$ , 0.18  $\rightarrow$  0.09  $\mu\text{m}$ ).

**3.3. Mechanism for the Formation of Spherical Assemblies.** Why do spherical assemblies form upon slow diffusion of nonsolvents, and why do only limited alternating copolymers assemble into such well-shaped spheres? From our results, spherical assemblies tend to form when polar

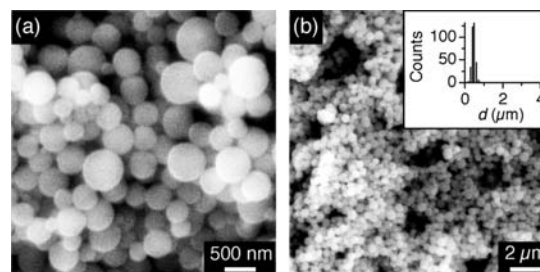


**Figure 4.** SEM micrographs of an air-dried  $\text{CHCl}_3/\text{MeOH}$  suspension of the spherical assemblies of **F8EDOT**, prepared in a wide-mouth Petri dish. Inset in (b) shows histogram of the diameters of the spherical assemblies of **F8EDOT**, prepared in a wide-mouth Petri dish. The number of sample is 350.

nonsolvents such as MeOH and acetone are diffused into the polymer solution. These nonsolvents have low affinity with the hydrophobic polymers having linear or branched aliphatic chains. As the result, the polymers possibly aggregate while minimizing the contact area with the polar nonsolvent, thereby gradually growing into a spherical geometry as thermodynamic products. In fact, simple evaporation of the solvent from the  $\text{CHCl}_3$  solution of **F8EDOT** hardly yielded spheres but only gave an amorphous film (Figure S14a). On the other hand, when MeOH was added in advance to the  $\text{CHCl}_3$  solution of **F8EDOT** ( $\text{CHCl}_3/\text{MeOH} = 10/1$  v/v), and the resultant suspension was heated to dissolve the polymer and then aged at  $25^\circ\text{C}$ , precipitation readily resulted within several minutes. However, the resultant precipitates were ill-shaped and fused spheres (Figure S14b). Therefore, slow diffusion of polar nonsolvent is one of important factors to yield well-shaped spheres. In colloidal sciences, amphiphilicity with large headgroup and small tail group is one of the driving forces for spherical assemblies.<sup>17–19,34–36</sup> However, in the present case, copolymers we utilized do not possess such amphiphilicity. Instead, polarity of good and nonsolvents plays a crucial role for the colloidal formation.

Crystallinity of polymers is another important factor. Polymers possessing high rigidity or interchain crystallinity tend to crystallize anisotropically, which disturb the assembly into isotropic spherical geometry. In fact, **RR-P3HT** having high interchain crystallinity<sup>23,24,37,38</sup> hardly formed discrete assemblies but only gave irregular aggregates (Figure S4), whereas **rr-P3HT** having low interchain crystallinity due to the random regularity of the hexyl chains formed pseudospherical structures (Figure S5). Furthermore, in case of **F8TMT2** and **F8T2**, the former formed well-shaped spheres (Figure 1), while the latter gave only ill-defined aggregates (Figure S6). Because four methyl groups on the bithiophene moiety in **F8TMT2** disturb a planarity of the polymer, polymer backbone most likely forms twisted configurations, leading to disordered interchain packing.<sup>39</sup> On the other hand, **F8T2** possesses much planar structure, which enhances the interchain crystallinity.<sup>40</sup> Copolymers **F8BT** and **PCPDTBT** also form spheres, but they are not quantitative and not well-shaped, possibly due to the rather high interchain crystallinity.<sup>41,42</sup>

We conducted X-ray diffraction (XRD) experiments to confirm differences of the crystallinity (Figure S15). However, except for **RR-P3HT**, diffraction peaks were hardly attained for all samples by conventional XRD studies, because long-range structural ordering of  $\pi$ -conjugated polymers is generally achieved by postannealing of polymer films.<sup>21,23,24</sup> Instead, photoemission spectra showed clear differences, giving important indication on their  $\pi$ -conjugation.  $\text{CHCl}_3$  solutions of **F8T2** and **F8TMT2** show maximum photoluminescence peaks ( $\lambda_{\text{PLmax}}$ ) of 499 and 468 nm, respectively, indicating that **F8T2** has the larger  $\pi$ -conjugation length than **F8TMT2** due to the high planarity of the polymer even in solution. The fluorescence spectra of the drop-cast film from  $\text{CHCl}_3$  solution of **F8T2** exhibited significant red shift ( $\Delta\lambda_{\text{PLmax}} = 42$  nm), and irregular aggregates of **F8T2** afforded by slow precipitation showed further red-shifted fluorescence ( $\Delta\lambda_{\text{PLmax}} = 46$  nm, Figure 5a, broken lines, and b). These results indicate that either expansion of the intrachain  $\pi$ -conjugation or interchain  $\pi$ -electronic interaction, or both of these, takes place in the solid state. In contrast,  $\lambda_{\text{PLmax}}$  of the cast film of the spheres of **F8TMT2** (475 nm,  $\Delta\lambda_{\text{PLmax}} = 7$  nm), as well as that formed from  $\text{CHCl}_3$  solution of **F8TMT2** (474 nm,  $\Delta\lambda_{\text{PLmax}} = 6$  nm),

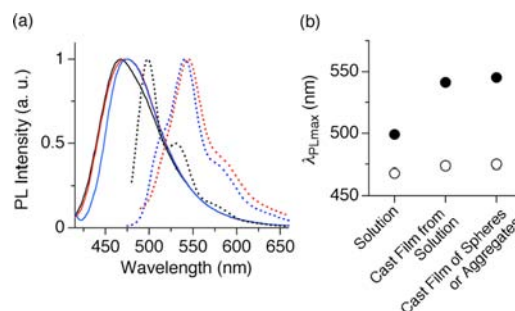


**Figure 5.** (a) Photoluminescence spectra of **F8TMT2** (solid lines) and **F8T2** (broken lines) for  $\text{CHCl}_3$  solutions (black), cast film from the solutions (blue), and cast film of the self-assembled precipitates (red). The excitation wavelengths are 368 and 371 nm for solution and films of **F8TMT2**, respectively, and 457 and 454 nm for solution and films of **F8T2**, respectively. (b) Plots of  $\lambda_{\text{PLmax}}$  of **F8TMT2** (○) and **F8T2** (●) for  $\text{CHCl}_3$  solution, drop-cast film from the solution, and cast films of spheres (**F8TMT2**) or aggregates (**F8T2**).

were not so much shifted from  $\lambda_{\text{PLmax}}$  of the solution of **F8TMT2** (Figure 5a, solid lines, and b). These results clearly indicate that neither expansion of intrachain  $\pi$ -conjugation nor interchain  $\pi$ -electronic interaction take place in the solid films of **F8TMT2**, irrespective of whether the aggregation takes place kinetically (solution-cast) or thermodynamically (spheres). Concerning **F8EDOT**, a certain red shift of  $\lambda_{\text{PLmax}}$  was observed by the formation of spheres ( $\Delta\lambda_{\text{PLmax}} = 37$  nm, Figure S16), which was rather large in comparison with that of **F8TMT2** ( $\Delta\lambda_{\text{PLmax}} = 6$  nm) but not as large as that of **F8T2** ( $\Delta\lambda_{\text{PLmax}} = 46$  nm). We assume that the degree of steric hindrance of the ethylenedioxy moieties in **F8EDOT** is smaller than that of the methyl groups in **F8TMT2**, which results in the smaller twisting of the  $\pi$ -conjugation in **F8EDOT** than **F8TMT2**. These results also support the fact that **F8TMT2** easily forms well-defined spheres under various solvent combinations (Table 3), whereas **F8EDOT** forms spheres only in a limited solvent combination (Table 4).

**3.4. Optical and Photoconducting Properties.** Figure 6 shows electronic absorption and diffuse reflectance spectra of

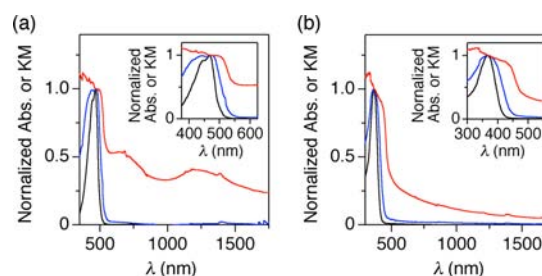


**Figure 6.** Normalized photoabsorption spectra of  $\text{CHCl}_3$  solutions (black) and their cast films (blue) and normalized Kubelka–Munk (KM) spectra of cast films of the self-assembled spheres (red) of **F8EDOT** (a) and **F8TMT2** (b).

**F8EDOT** and **F8TMT2** in solution and solid states. For both samples, a certain broadening of the absorption peaks was observed by the assembly of polymers (Figure 6, inset). In addition, for the spheres of **F8EDOT**, broad reflections were observed at the visible-to-NIR regions ( $\lambda \approx 700$  and  $1200$  nm, respectively, Figure 6a), which resulted from assembly of submicrometer sized colloids. On the other hand, no such selected reflections were observed in the NIR region for the

spherical assemblies of **F8TMT2**, because the spheres were large with several micrometers in diameter.

We found an interesting phenomenon that photocarrier lifetime is extremely enhanced by the formation of nanospheres. For evaluating lifetimes and transport properties of photocarriers, we employed a FP-TRMC,<sup>27</sup> which allows for probing the motion of photocarriers under a rapidly oscillating electric field. Because of this probing function, this technique does not require electrodes for charge injection, so that one can evaluate intrinsic dynamics of mobile carriers. Furthermore, under such high resonant frequency conditions, charge carriers can vibrate only in a nanoscale range.<sup>43</sup> Therefore, FP-TRMC transient maxima of the spheres are considered to reflect mostly the intrasphere carrier transport events.

Upon laser flash, rise and decay profiles of a TRMC signal, given by  $\phi\Sigma\mu$ , are observed, where  $\phi$  and  $\Sigma\mu$  represent photocarrier generation yield and sum of the mobilities of generated charge carriers, respectively. Figure 7a shows TRMC

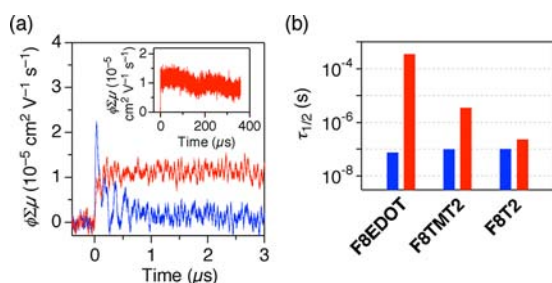


**Figure 7.** (a) FP-TRMC profiles of a thin film of the spheres of **F8EDOT** (red) and that drop-casted from  $\text{CHCl}_3$  solution (blue). Inset shows FP-TRMC profiles of a cast film of the spheres of **F8EDOT** with the longer time scale. (b) Lifetimes ( $\tau_{1/2}$ ) of charge carriers generated by laser excitation of **F8EDOT**, **F8TMT2**, and **F8T2** in thin films formed by drop-cast from their  $\text{CHCl}_3$  solutions (blue) and suspension of self-assembled spheres or aggregates (red).  $\tau_{1/2}$  is defined by the time when the FP-TRMC transient decays down to one-half of its maximum value.

profiles of cast films of **F8EDOT** in a spherical geometry (red) and drop-cast from its  $\text{CHCl}_3$  solution (blue). The maximum value of  $\phi\Sigma\mu$  ( $\phi\Sigma\mu_{\text{max}}$ ) of the spheres ( $1.1 \times 10^{-5} \text{ cm}^2 \text{ V}^{-1} \text{ s}^{-1}$ ) was reduced to 50% of that of the cast film from the solution ( $2.2 \times 10^{-5} \text{ cm}^2 \text{ V}^{-1} \text{ s}^{-1}$ ). These values were rather small because of the low charge-separation efficiencies ( $\phi$ ) in comparison with that of D/A mixture<sup>44</sup> and D/A molecular-layer heterojunction systems.<sup>45–47</sup> Of great interest, photocarrier lifetime ( $\tau_{1/2}$ ) was markedly enhanced by more than 3–4 orders of magnitude by the formation of spherical geometry (0.075 and  $>350 \mu\text{s}$  for cast film from solution and spherical assemblies, respectively, Figure 7b). A similar tendency was observed for **F8TMT2**, where  $\tau_{1/2}$  of the spheres was 35-fold enhanced in comparison with that of a cast film from the solution (Figures 7b and S17a). In sharp contrast, **F8T2**, which does not form spherical assemblies, showed only a moderate difference of  $\tau_{1/2}$  between the self-assembled aggregates and drop-cast film from its solution (2.3-fold, Figures 7b and S17b). We assume that such long-lived photocarriers in spherical assemblies possibly derive from the isolation of each photo-generated carrier, where intersphere charge recombination is effectively suppressed. Accordingly, spherical assemblies of **F8EDOT** exhibited the higher  $\tau_{1/2}$  value than that of **F8TMT2** having the larger diameters and irregularly aggregated **F8T2**. In

addition, the better interchain packing in **F8T2** possibly causes the prompt interchain charge recombination, which results in the shorter lifetime of photocarriers than that of the spherical assembly of **F8TMT2**. Similar tendency was also observed for our previous research on spherical and fibril assemblies from porphyrin–fullerene dyad, where the former exhibited nearly 3 orders of magnitude longer photocarrier lifetime (16 ms) than the latter (18  $\mu\text{s}$ ).<sup>48</sup> As the general tendency, self-assembled precipitates from  $\pi$ -conjugate polymers having discrete shape and finite size exhibited smaller  $\phi\Sigma\mu_{\text{max}}$  and longer  $\tau_{1/2}$  values than the cast films from their solutions (Table S8). The smaller  $\phi\Sigma\mu_{\text{max}}$  for the self-assembled precipitates results from the shorter conjugation length during the assembly process using polar nonsolvents, which are often observed for polymers with reprecipitation treatments.<sup>49</sup> Intersphere recombination may occur easily for the fused spheres, resulting in the shorter  $\tau_{1/2}$  than the discrete spheres. Photocarriers having long lifetime are quite advantageous for optoelectronic applications using spherical assemblies.

#### 4. CONCLUSION

We studied self-assembly of  $\pi$ -conjugated polymers upon slow precipitation from their solution. While most representative  $\pi$ -conjugated polymers hardly yielded spherical assemblies, some alternating copolymers assembled into well-shaped spherical structures quantitatively. The main factor for spherical assembly is attributed to the low crystallinity of the polymers, where copolymers with steric hindrance in their backbone and thereby having low crystallinity tend to form spheres. Optimizing the self-assembling conditions can systematically control size and deviation of the spheres. Photocarrier lifetimes in the spheres were markedly enhanced in comparison with that of the samples without forming spheres. More attempts are needed to create colloidal crystals such as precise control of the size and deviation, yet this research provides important knowledge for photonic applications using  $\pi$ -conjugated functional polymers.

#### ■ ASSOCIATED CONTENT

##### Supporting Information

Materials and measurements, synthesis, self-assembly, SEM, XRD, photoemission, and FP-TRMC. This material is available free of charge via the Internet at <http://pubs.acs.org>.

#### ■ AUTHOR INFORMATION

##### Corresponding Author

yamamoto@ims.tsukuba.ac.jp

##### Notes

The authors declare no competing financial interest.

#### ■ ACKNOWLEDGMENTS

We acknowledge Prof. Yoshikazu Suzuki of the University of Tsukuba, Japan, for XRD experiments and Dr. Qingmin Ji and Dr. Katsuhiko Ariga of the National Institute for Materials Science (NIMS), Japan, for SEM measurements. This work was partly supported by a Grant-in-Aid for Young Scientist B (23750144) from the Ministry of Education, Culture, Sports, Science and Technology, Japan, Industrial Technology Research Grant Program in 2011 from New Energy and Industrial Technology Development Organization (NEDO) of Japan, Cooperative Research Program of “Network Joint Research Center for Materials and Devices”, Shimadzu Science



and Technology Promotion Foundation, and Asahi Glass Foundation.

## REFERENCES

- (1) Oh, M.; Mirkin, C. A. *Nature* **2005**, *438*, 651–654.
- (2) Acharya, S.; Hill, J. P.; Ariga, K. *Adv. Mater.* **2009**, *21*, 2959–2981.
- (3) Galisteo-López, J. F.; Ibisate, M.; Sapienza, R.; Froufe-Pérez, L. S.; Blanco, Á.; López, C. *Adv. Mater.* **2011**, *23*, 30–69.
- (4) Fudouji, H. *Sci. Technol. Adv. Mater.* **2011**, *12*, 064704.
- (5) Pelaz, B.; Jaber, S.; de Aberasturi, D. J.; Wulf, V.; Aida, T.; de la Fuente, J. M.; Feldman, J.; Gaub, H. E.; Josephson, L.; Kagan, C. R.; Kotov, N. A.; Liz-Marzán, L. M.; Mattoussi, H.; Mulvaney, P.; Murray, C. B.; Rogach, A. L.; Weiss, P. S.; Willner, I.; Parak, W. J. *ACS Nano* **2012**, *6*, 8468–8483.
- (6) Kanai, T.; Sawada, T.; Toyotama, A.; Kitamura, K. *Adv. Funct. Mater.* **2005**, *15*, 25–29.
- (7) Molinos-Gómez, A.; Maymó, M.; Vidal, X.; Velasco, D.; Martorell, J.; López-Calahorra, F. *Adv. Mater.* **2007**, *19*, 3814–3818.
- (8) Furumi, S.; Kanai, T.; Sawada, T. *Adv. Mater.* **2011**, *23*, 3815–3820.
- (9) Sato, S.; Kajii, H.; Kawagishi, Y.; Fujii, A.; Ozaki, M.; Yoshino, K. *Jpn. J. Appl. Phys.* **1999**, *38*, L1475–L1477.
- (10) Polson, R. C.; Chipouline, A.; Vardeny, Z. V. *Adv. Mater.* **2001**, *13*, 760–764.
- (11) Deutsch, M.; Vlasov, Y. A.; Norris, D. J. *Adv. Mater.* **2000**, *12*, 1176–1180.
- (12) Yabu, H.; Tajima, A.; Higuchi, T.; Shimomura, M. *Chem. Commun.* **2008**, 4588–4589.
- (13) John, S.; Quang, T. *Phys. Rev. Lett.* **1997**, *78*, 1888–1891.
- (14) Yoshino, K.; Tatsuahara, S.; Kawagishi, Y.; Ozaki, M.; Zakhidov, A. A. *Appl. Phys. Lett.* **1999**, *74*, 2590–2592.
- (15) Pecher, J.; Mecking, S. *Chem. Rev.* **2010**, *110*, 6260–6279.
- (16) Kuehne, A. J. C.; Gather, M. C.; Sprakel, J. *Nat. Commun.* **2012**, *3*, 1088.
- (17) Alam, M. M.; Zhu, Y.; Jenekhe, S. A. *Langmuir* **2003**, *19*, 8625–8628.
- (18) Jenekhe, S. A.; Chen, X. L. *Science* **1998**, *279*, 1903–1907.
- (19) Jenekhe, S. A.; Chen, X. L. *J. Phys. Chem. B* **2000**, *104*, 6332–6335.
- (20) Chen, X. L.; Jenekhe, S. A. *Macromolecules* **2000**, *33*, 4610–4612.
- (21) Beaujuge, P. M.; Fréchet, J. M. J. *J. Am. Chem. Soc.* **2011**, *133*, 20009–20029.
- (22) Kim, F. S.; Ren, G.; Jenekhe, S. A. *Chem. Mater.* **2011**, *23*, 682–732.
- (23) Sirringhaus, H.; Brown, P. J.; Friend, R. H.; Neilsen, M. M.; Bechgaard, K.; Langeveld-Voss, B. M. W.; Spiering, A. J. H.; Janssen, R. A. J.; Meijer, E. W.; Herwig, P.; de Leeuw, D. M. *Nature* **1999**, *401*, 685–688.
- (24) Yang, X.; Loos, J.; Veenstra, S. C.; Verhees, W. J. H.; Wienk, M. W.; Kroon, J. M.; Michels, M. A. J.; Janssen, R. A. J. *Nano Lett.* **2005**, *5*, 579–583.
- (25) Fujinami, Y.; Kuwabara, J.; Lu, W.; Hayashi, H.; Kanbara, T. *ACS Macro Lett.* **2012**, *1*, 67–70.
- (26) Yamazaki, K.; Kuwabara, J.; Kanbara, T. *Macromol. Rapid Commun.*, in press, DOI: 10.1002/marc.201200550.
- (27) Saeki, A.; Seki, S.; Takenobu, T.; Iwasa, Y.; Tagawa, S. *Adv. Mater.* **2008**, *20*, 920–923.
- (28) Friend, R. H.; Gymer, R. W.; Holmes, A. B.; Burroughes, J. H.; Marks, R. N.; Taliani, C.; Bradley, D. D. C.; Dos Santos, D. A.; Brédas, J. L.; Lögdlund, M.; Salaneck, W. R. *Nature* **1999**, *397*, 121–128.
- (29) Donat-Bouillud, A.; Lévesque, I.; Tao, Y.; D'Iorio, M. *Chem. Mater.* **2000**, *12*, 1931–1936.
- (30) Sirringhaus, H.; Kawase, T.; Friend, R. H.; Shimoda, T.; Inbasekaran, M.; Wu, W.; Woo, E. P. *Science* **2000**, *290*, 2123–2126.
- (31) Kim, Y.; Cook, S.; Choulis, S. A.; Nelson, J.; Durrant, J. R.; Bradley, D. D. C. *Chem. Mater.* **2004**, *16*, 4812–4818.
- (32) Mühlbacher, D.; Scharber, M.; Morana, M.; Zhu, Z.; Waller, D.; Gaudiana, R.; Brabec, C. *Adv. Mater.* **2006**, *18*, 2884–2889.
- (33) Kim, J. Y.; Lee, K.; Coates, N. E.; Moses, D.; Nguyen, T.-Q.; Dante, M.; Heeger, A. J. *Science* **2007**, *317*, 222–225.
- (34) Fujita, N.; Yamashita, T.; Asai, M.; Shinkai, S. *Angew. Chem., Int. Ed.* **2005**, *44*, 1257–1261.
- (35) Koizumi, Y.; Seki, S.; Tsukuda, S.; Sakamoto, S.; Tagawa, S. *J. Am. Chem. Soc.* **2006**, *128*, 9036–9037.
- (36) Nakanishi, T.; Michinobu, T.; Yoshida, K.; Shirahata, N.; Ariga, K.; Möhwald, H.; Kurth, D. G. *Adv. Mater.* **2008**, *20*, 443–446.
- (37) Ihn, K. J.; Moulton, J.; Smith, P. J. *Polym. Sci., Part B: Polym. Phys.* **1993**, *31*, 735–742.
- (38) Kim, Y.; Cook, S.; Tuladhar, S. M.; Choulis, S. A.; Nelson, J.; Durrant, J. R.; Bradley, D. D. C.; Giles, M.; McCulloch, I.; Ha, C.-S.; Ree, M. *Nat. Mater.* **2006**, *5*, 197–203.
- (39) Kuwabara, J.; Nohara, Y.; Choi, S. J.; Fujinami, Y.; Lu, W.; Yoshimura, K.; Oguma, J.; Suenobu, K.; Kanbara, T. *Polym. Chem.*, in press, DOI: 10.1039/C2PY20917A.
- (40) Werzer, O.; Resel, R.; Chernev, B.; Plank, H.; Rothmann, M. M.; Strohmriegel, P.; Trimmel, G.; Rapallo, A.; Porzio, W. *Carbon* **2011**, *52*, 3368–3373.
- (41) Zhang, M.; Tsao, H. N.; Pisula, W.; Yang, C.; Mishra, A. K.; Müllen, K. *J. Am. Chem. Soc.* **2007**, *129*, 3472–3473.
- (42) Tsao, H. N.; Cho, D.; Andreasen, J. W.; Rouhanipour, A.; Breiby, D. W.; Pisula, W.; Müllen, K. *Adv. Mater.* **2009**, *21*, 209–212.
- (43) Amaya, T.; Seki, S.; Moriuchi, T.; Nakamoto, K.; Nakata, T.; Sakane, H.; Saeki, A.; Tagawa, S.; Hirao, T. *J. Am. Chem. Soc.* **2009**, *131*, 408–409.
- (44) Saeki, A.; Tsuji, M.; Seki, S. *Adv. Energy Mater.* **2011**, *1*, 661–669.
- (45) Yamamoto, Y.; Fukushima, T.; Saeki, A.; Seki, S.; Tagawa, S.; Ishii, N.; Aida, T. *J. Am. Chem. Soc.* **2007**, *129*, 9276–9277.
- (46) Yamamoto, Y.; Zhang, G.; Jin, W.; Fukushima, T.; Ishii, N.; Saeki, A.; Seki, S.; Tagawa, S.; Minari, T.; Tsukagoshi, K.; Aida, T. *Proc. Natl. Acad. Sci. U.S.A.* **2009**, *106*, 21051–21056.
- (47) Charvet, R.; Yamamoto, Y.; Sasaki, T.; Kim, J.; Kato, K.; Takata, M.; Saeki, A.; Seki, S.; Aida, T. *J. Am. Chem. Soc.* **2012**, *134*, 2524–2527.
- (48) Hizume, Y.; Tashiro, K.; Charvet, R.; Yamamoto, Y.; Saeki, A.; Seki, S.; Aida, T. *J. Am. Chem. Soc.* **2010**, *132*, 3292–3294.
- (49) Saeki, A.; Fukumatsu, T.; Seki, S. *Macromolecules* **2011**, *44*, 3416–3424.